2021

Direct Selective Laser Synthesis of CuCrFeNiTiAl High Entropy Alloy from Elemental Powders through Selective Laser Melting

Joni Dhar
The University of Texas Rio Grande Valley

Lazaro Lopez
The University of Texas Rio Grande Valley

Shanshan Zhang
The University of Texas Rio Grande Valley

Ben Xu

Mohammed Jasim Uddin
The University of Texas Rio Grande Valley

See next page for additional authors

Solid Freeform Fabrication 2021: Proceedings of the 32nd Annual International
Solid Freeform Fabrication Symposium – An Additive Manufacturing Conference
Reviewed Paper

Direct Selective Laser Synthesis of CuCrFeNiTiAl High Entropy Alloy from Elemental Powders through Selective Laser Melting

Joni Dhar[1], Lazaro Lopez[1], Shanshan Zhang[1], Ben Xu[2], Jasim Uddin[1], Jianzhi Li[1]

[1]Manufacturing and Industrial Engineering, University of Texas Rio Grande Valley, Edinburg, TX 78539
[2]Mechanical Engineering, Mississippi State University, Mississippi State, MS, 39762

Abstract

This study investigated the synthesis of CuCrFeNiTiAl high entropy alloy (HEA) from pure elements using selective laser melting (SLM). The objectives are to validate the feasibility of the HEA fabrication from elemental powder materials, and to examine the effect of various process conditions in SLM, such as laser power, point distance and laser exposure time, on the microstructures formed. The as-built samples under high, medium and low energy densities were characterized by X-ray diffraction (XRD), and the microstructures were observed using scanning electron microscopy (SEM). The XRD results showed that five major crystal structure phases (hexagonal, monoclinic, orthorhombic, body-centered cubic and rhombohedral) were present in all samples. Fine-grained phases were noticed on the sample surface with non-uniform microstructural distribution. Such phases in high and low energy density samples were observed polygonal while round-shaped microstructures were observed for samples prepared under medium energy density conditions. Also, the grain size was proportional to energy levels of the fabrication process. Large size and clustered structures are prominent in samples produced under high energy density.

Keywords: selective laser melting, high entropy alloy, microstructure, additive manufacturing

1. Introduction

High-entropy alloys (HEA) as a new family of alloys are composed of five or more principal elements in equimolar or near-equimolar concentrations [1, 2]. HEAs contain principal elements with concentration between 5 to 35 at %, and minor elements each below 5 at % [2]. By combining multiple elements in an alloy system, HEAs are showing a great possibility for designing novel materials with superior properties expected under extreme operating conditions (high temperature, high pressure, etc.) in many applications in the defense and energy industries such as nuclear reactors, missiles, jet engine, nozzle, turbine blade, compressor blade of aero engine, etc.

The earliest attempts to design high entropy alloys are the research works of two research groups led by Prof. B. Cantor and Prof. J.W. Yeh in 2004 [3, 4]. Both the groups investigated multicomponent alloy systems, which triggered the development of high entropy alloy. Yeh is the first who thoroughly described four core effects of high entropy alloys: high-entropy effect, lattice distortion, sluggish diffusion, and cocktail effect [5]. High-entropy effect tends to stabilize the HEA phase by minimizing the Gibbs free energy. Severe lattice distortion effect describes the displacement of lattice sites in HEA system from the perfect crystal lattice site. Sluggish diffusion

effect explains how the disorder of the multi-component HEA phase causes the local lattice potential energy to form deep traps that inhibit diffusion among the elements. Cocktail effect is the selection of the specific elements with specific properties that will contribute to the desired properties of the final high-entropy system.

Following the above-mentioned pioneering works, researchers have studied many HEA systems. CuCrFeCoNiAl [6-9] and its Cu free derivations [10, 11] are the most comprehensively studied alloy systems among all the HEA systems reported. One of the important derivatives is CuCrFeNiTiAl where Co is replaced by Ti. As titanium has the highest negative mixing enthalpy with rest of the elements, inclusion of titanium in HEA system causes different intermetallic phases to grow. These phases strengthen HEA with improved strength and hardness [12, 13]. Besides, the solid solution strengthening mechanism of titanium, due to its higher atomic radius, enhances strength of alloys greatly[13]. Therefore, CuCrFeNiTiAl HEA system have a high potential of creating HEAs with promising performance.

With the growing interest in research on HEA, many HEA fabrication systems have been invented such as arc melting, plasma arc sintering, casting, etc. [14-18]. Unlike conventional manufacturing techniques, powder-bed additive manufacturing (AM), such as selective laser melting (SLM) process, has been investigated for HEA fabrication [19, 20]. Studies were reported in literature focusing on the effect of printing parameters (laser power, hatch distance, point distance, exposure time, laser focus diameter, scanning rotation angle, etc.) on the microstructure and properties of alloys made by SLM process [21-23]. However, the reported feedstock of these SLM fabricated HEAs are mostly based on pre-alloyed powders [24], which show disadvantages such as high cost, and lack of flexibility of material designs.

The objective of this study is to demonstrate the feasibility of HEA fabrication from elemental powders via SLM process, and to examine the effect of different process parameters in SLM, including laser power, exposure time, and point distance, on the microstructures of the specimens. A CuCrFeNiTiAl high entropy alloy system was synthesized directly from elemental powders under different energy densities. Then, the as-built specimens were characterized using X-ray diffraction (XRD) for crystal structures and observed under scanning electron microscopy (SEM).

2. Experimental details

2.1. Materials

The CuCrFeNiTiAl HEA powder was blended using 99.9 % pure (trace metal basis) Cu, Cr, Fe, Ni, Ti and Al elemental powders, supplied by Sigma-Aldrich Co. The nominal composition of the powder blend is given in **Table 1**. The elemental powders were measured and mixed in an oxygen-free sealed chamber filled with argon (Ar) atmosphere and then placed into a V-type blender rotating for 2 hours at 200 rpm.

Table 1. Chemical composition of the powder blend.

Element	Al	Cu	Cr	Fe	Ni	Ti
Weight, %	2.50	22.36	18.20	19.59	20.61	16.72
Molar Ratio, %	5	19	19	19	19	19

2.2. SLM Fabrication

A Renishaw AM 250 SLM system was used for fabricating the samples using the blended HEA powder. This system utilizes a high precision fiber laser with 1070 nm wavelength, 70 µm focal diameter and 200 W power. The laser scanned the powder surface during the SLM process in pulsed mode. The duration of heating by the laser at a single point is called exposure time and the distance between two consecutive points along a hatch line is called point distance. Hatch spacing is defined as the distance between two consecutive hatch lines. To save the powder materials and build time, a reduced build volume (RBV) system was developed, as shown in **Figure 1**. The build substrate is customized and machined using 316L stainless steel with a dimension of 50.8 mm × 50.8 mm. To investigate the effect of different process conditions on the microstructure of the synthesized CuCrFeNiTiAl samples, a 5 × 5 test series was designed with different process parameter combinations. Each sample in the test series was designed as a thin square chip with the dimension of 6.4 mm × 6.4 mm × 0.84 mm. The size of substrate in the RBV system was considered during the selection of this dimension.

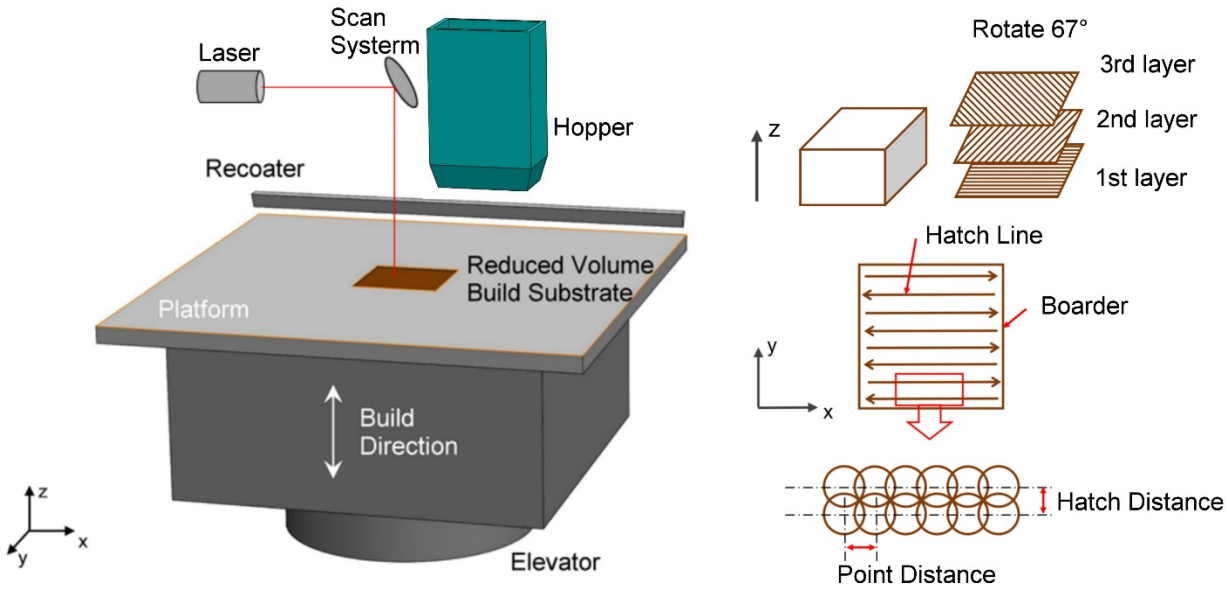

Figure 1. Reduced build volume system used in this work.

In this study, the process parameters were investigated, including laser power, exposure time, and point distance, as shown in **Table 2**. The hatch spacing and layer thickness were kept constant at 90 µm and 70 µm, respectively. A unidirectional meander build strategy was applied with an alternative rotation of 67° in the consecutive layers. The prescribed parameters, such as laser beam size and laser focus offset were used the machine default setting. During the fabrication, the oxygen concentration inside the chamber was set 500 ppm (parts per million) and high purity argon gas with a line pressure of 1 bar was used as inert media. For facilitating proper melting of the first powder layer, the build substrate was preheated to 170 °C. When the process chamber was ready, the HEA powder blend was spread using the in-house developed RBV system.

Table 2. Experimental design of the 5 × 5 test series.

Point Distance (μm) →		60	55	50	45	40
Power (W)↓	Exposure Time (μs)↓					
100	20	1A	1B	1C	1D	1E
125	35	2A	2B	2C	2D	2E
150	50	3A	3B	3C	3D	3E
175	65	4A	4B	4C	4D	4E
200	80	5A	5B	5C	5D	5E

According to Gu and Shen [25], the energy density (*ED*) can be calculated in terms of laser power (*P*), scan speed (*v*), hatch spacing (*h*) and layer thickness (*l*). However, in the Renishaw AM250 system, the scan speed of the pulsed laser is determined by the ratio of point distance (*d*) and exposure time (*t*). Therefore, the energy density in this study is evaluated by Equation (1). In this study, three samples under high, medium and low energy densities were selected, marked as 1A, 3C and 5E in **Figure 2**. Per Equation (1), the energy densities for Samples 1A, 3C and 5E are 5.29 kJ/mm^3, 23.81 kJ/mm^3, and 63.49 kJ/mm^3, respectively as shown in **Table 3**.

$$ED = \frac{P \cdot t}{d \cdot h \cdot l} \tag{1}$$

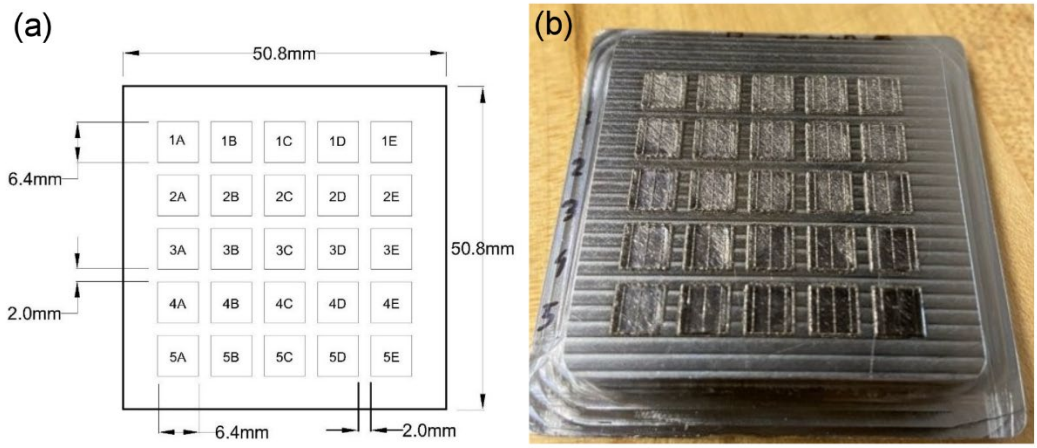

Figure 2. (a) Detailed dimension of the test series, and (b) SLM fabricated samples.

Table 3. Energy densities (kJ/mm^3) of test series.

Point Distance (μm) →		60	55	50	45	40
Power (W)↓	Exposure Time (μs)↓					
100	20	5.29	5.77	6.35	7.05	7.94
125	35	11.57	12.63	13.89	15.43	17.36
150	50	19.84	21.65	23.81	26.46	29.76
175	65	30.09	32.83	36.11	40.12	45.14
200	80	42.33	46.18	50.79	56.44	63.49

2.3. Testing methods

The as-built samples were evaluated to study the phase structures by the X-ray diffraction (XRD). A Bruker D8 X-ray diffractometer with a Cu K_α radiation (wavelength, $\lambda = 1.5406$ Å) was operated at 40 kV voltage with the current of 40 mA to identify phase structures. The radiation scanned sample surfaces continuously with a locked coupled step size of 0.01°, a speed of 1.17° min^{-1} and 2θ between 10° and 80°. The XRD profiles were then analyzed by Crystallographica Search-Match (CSM) program developed by Oxford Cryosystems [26]. To characterize morphology and microstructures, images on the surface of the blocks were taken using Carl Zeiss Sigma VP Scanning Electron Microscope (SEM). Average length, point distance and area of bright phases found on SEM images on nanoscale were calculated using ImageJ software developed by National Institute of Health (NIH). Energy Dispersive X-ray Spectroscopy (EDX) detector on the SEM model was used to identify the composition weight and atomic ratio of metal elements available in different samples. No special preparation was needed for the testing of electrically conductive HEA samples and separation of the samples from the substrate was not required.

3. Results and Discussion

3.1. XRD Analysis

The XRD measurements were carried out to examine the crystal structures of the SLM as-built CuCrFeNiTiAl HEA samples. **Figure 3** shows the XRD patterns of the samples under various energy densities.

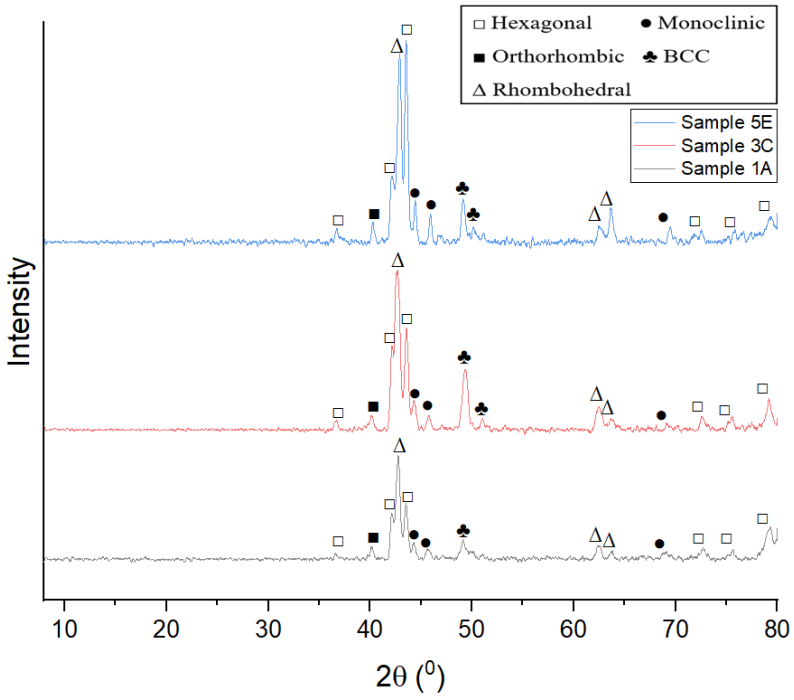

Figure 3. XRD patterns of CuCrFeNiTiAl HEA samples under different energy densities.

3.2. Microstructure analysis

All XRD plots have been corrected for background noise and five strong peaks are visible in the 2θ range from 10° to 80°. The result shows that all three samples consist of five different crystal phases: hexagonal, orthorhombic, monoclinic, body-centered cubic (BCC), and rhombohedral. The alloy system comprises a major hexagonal solid solution matrix. Two major peaks are found at 2θ at 42.63°-42.85° and 43.52°-43.56° with rhombohedral and hexagonal crystal structures, respectively. High peaks responsible for rhombohedral structure in low, medium and high energy density areas, with intensities of 222 (2θ = 42.78°), 282 (2θ = 42.63°), 383 (2θ = 42.85°) respectively. Similarly, for hexagonal structure indicating high peaks in all three areas, respective intensities are 127 (2θ = 43.52°), 210 (2θ = 43.56°), and 404 (2θ = 43.54°). With increasing energy input during the laser melting process, the intensity of major XRD peaks and other minor peaks have increased. However, the peak identified for BCC phase has higher intensity at mid-energy density area sample compared to high and low energy density area samples.

Figure 4(a) shows an example of low magnification SEM pictures of the CuCrFeNiTiAl samples. It can be noticed that the surface morphology shows non-uniform microstructural distribution, which is considered due to the blending procedure. Additionally, though most of the high entropy alloy systems developed using casting process exhibit dendritic structural morphology, the CuCrFeNiTiAl samples in this study exhibited fine grained structures.

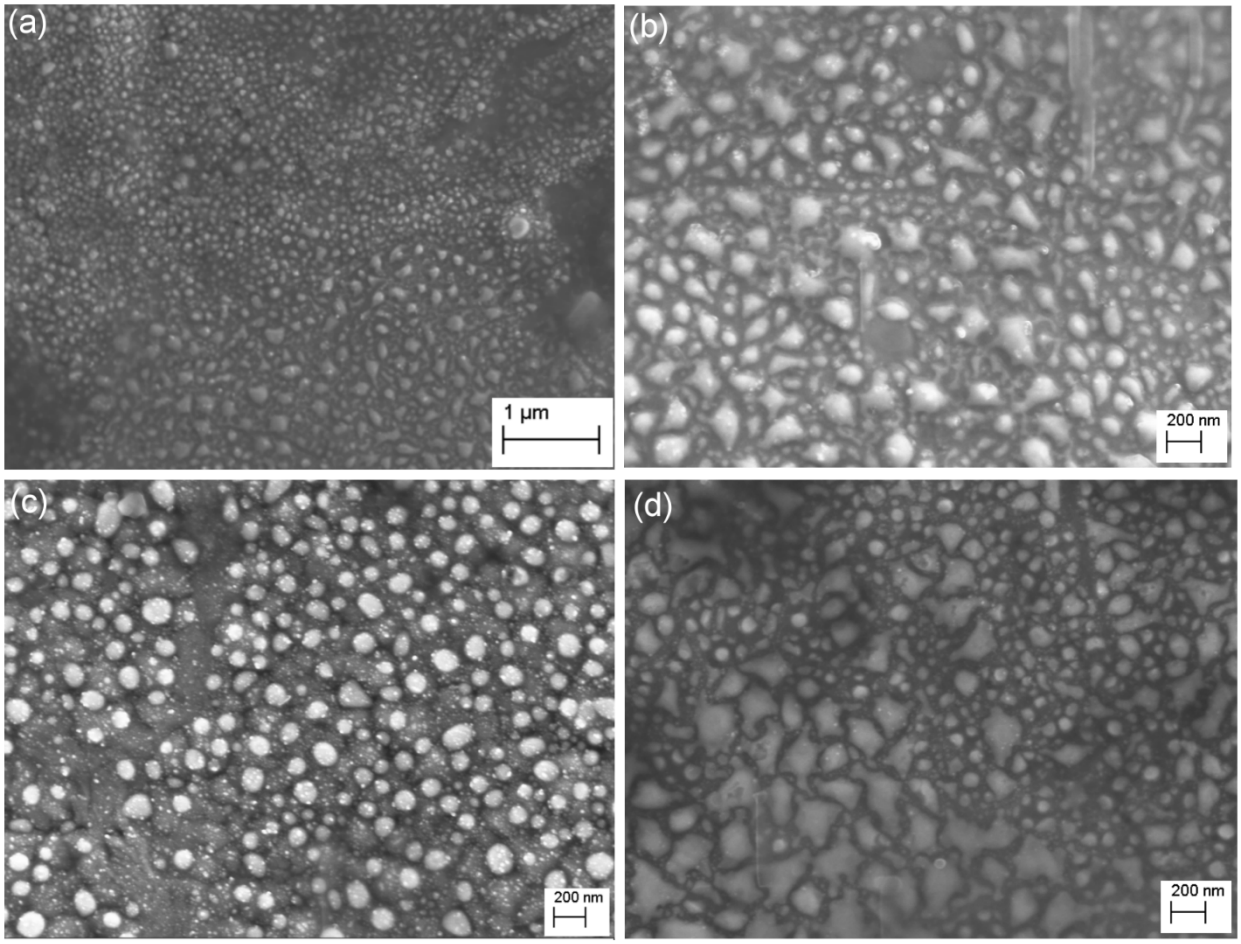

Figure 4. SEM pictures of CuCrFeNiTiAl sample of (a) 3C at low magnification; and samples of (b) 1A, (c) 3C, and (d) 5E at high magnification.

High magnification pictures of the samples were taken in specific regions of interest and multi-phase morphology was observed, as shown in **Figure 4(b-d)**. The two distinct structures identified as bright area and dark area, with noticeable difference in shape, size and distribution. The amount of the bright phases shows increasing with an increase of energy density. In addition, it was observed that the bright phases in Sample 1A and 5E have polygonal shape while round-shaped bright phase was observed in sample 3C.

Average length, point distance and area of bright phases are calculated using ImageJ software. The mean length of the bright phase is the largest in the high energy density area (Sample 5E) which is 186.24 nm and the smallest mean length is 122.92 nm which is found in the medium energy density area (Sample 3C). The mean area of bright phases has increased with increasing laser energy input during melting from 8989.82 nm^2 through 12857.71 nm^2 to 13016.14 nm^2. The point distances are measured to depict the distribution of bright phases throughout the microstructure. It is found that comparing to other two samples, the bright phases are positioned more closely in sample 5E with a mean point distance of 93.72 nm.

3.3. EDX Element Analysis

EDX analysis was conducted for Samples 1A, 3C, and 5E to find out elemental compositions in both bright and dark areas upon different energy densities. **Table 4** shows the composition of metal elements from EDX analysis given at weight percentage. **Figure 5** shows the comparison of chemical composition in both bright and dark areas of the three samples with their nominal compositions. It is noticed that the EDX analyzed composition of each element was significantly different away from the nominal composition ratio, even though the elemental powder materials were pre-blended in equimolar ratio except for Al. Among all the principal elements, Cr has the lowest molar ratio and the highest molar ratio is observed in case of Ti. The molar ratio of Cr, Fe and Ni are lower than the nominal molar ratio (19 %), and Ti is about twice amount of the nominal values. However, Cu is the only principal element whose presence in different sample areas is consistent with the nominal molar ratio. In all samples, the molar ratio of Al is slightly greater than 5 %.

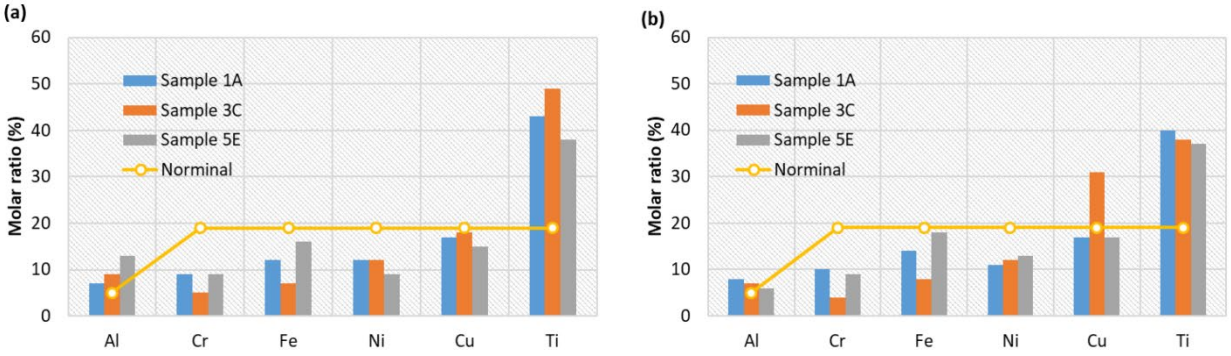

Figure 5. Chemical composition of (a) bright area and (b) dark area of CuCrFeNiTiAl samples.

When comparing between the bright and dark areas, a significant difference is noticed in Sample 3C that the bright area of Sample 3C shows rich of Ti element, while Cu is rich in dark area. This elemental segregation can be explained by mixing enthalpy of principal elements. As

Cu has higher mixing enthalpy with other elements and mixing enthalpy of Ti is very low, Cu is repelled from the Ti-rich bright area [27].

Moreover, though principal elements were mixed in equimolar ratio, the EDX analysis of the CuCrFeNiTiAl sample fabricated in SLM process found no equimolar ratio in any sample in this study. It can be indicated that insufficient energy was deposited into the powder blend. The energy generated from laser during melting was from 5.29 KJ/mm^3 to 63.49 KJ/mm^3 and depending on the absorption rate of heat by the powder mixture, a portion of that energy is utilized for melting which might have not become sufficient enough heat to melt powder completely. Another reason was that the rapid cooling of the melt pool was not able to provide sufficient time window for the diffusion of the elements to form random solid solution.

Table 4. Chemical composition of CuCrFeTiNiAl2.5 alloys in bright and dark areas.

	Al	Cr	Fe	Ni	Cu	Ti	Total
Block 1A							
Nominal	0.05	0.19	0.19	0.19	0.19	0.19	1.00
Bright	0.07	0.09	0.12	0.12	0.17	0.43	1.00
Dark	0.08	0.10	0.14	0.11	0.17	0.40	1.00
Block 3C							
Nominal	0.05	0.19	0.19	0.19	0.19	0.19	1.00
Bright	0.09	0.05	0.07	0.12	0.18	0.49	1.00
Dark	0.07	0.04	0.08	0.12	0.31	0.38	1.00
Block 5E							
Nominal	0.05	0.19	0.19	0.19	0.19	0.19	1.00
Bright	0.13	0.09	0.16	0.09	0.15	0.38	1.00
Dark	0.06	0.09	0.18	0.13	0.17	0.37	1.00

4. Conclusion

This study was intended to fabricate CuCrFeNiTiAl high entropy alloy by SLM process directly from the blend of six elemental powder materials. A sample matrix was produced on a 50.8 mm × 50.8 mm customized stainless-steel substrate, using different laser power and scan speed via full factorial experimental design. Three representative samples were selected for analysis and comparison in the as-built status. These three selected samples were then characterized using XRD, to study crystal structures, and using SEM and EDX to study the microstructures and elemental composition respectively. The conclusions drawn based on the investigation can be summarized as below:

(1) Five crystal structures were observed in the SLM-fabricated CuCrFeNiTiAl alloy samples including: hexagonal, orthorhombic, monoclinic, BCC, and rhombohedral. Thereinto, two major peaks appeared on the XRD graphs were found responsible for rhombohedral and hexagonal structures at angles of 42.63° and 43.56°, respectively.

(2) Through SEM observation at a low magnification, the samples exhibited non-uniform microstructural distribution which might be caused during the blending process.

(3) At a high magnification of SEM, the microstructures in three samples appear fine-grained bright phases dispersed on dark phases.

(4) Shape, size and distribution of bright phases have a significant correlation with laser energy density under different printing parameters. While round-shaped bright phases in the sample using medium energy density had the smallest grain size, sizes of polygonal grains in the samples with low and high energy densities were comparatively higher. The total area of bright phases increased with increasing energy input and the bright phases were most closely clustered in high energy density sample.
(5) Though mixed in equimolar ratio, no equal compositions of the five principal elements were obtained based on EDX results, indicating incomplete diffusion during melting and solidification process.

The multiple crystal structures observed in the samples strongly suggest that the heating process from the laser source was insufficient to create a time window that allows for full diffusion of the principal elements, and therefore, desired random solid solution was not obtained. Future research is suggested to investigate new laser scan strategy, and/or incorporating other heating mechanism to elongate the time of the liquid state of melt pool, thus allowing sufficient diffusion among the elements to form random solid solutions.

Acknowledgement

This study is financially supported by the Department of Defense (DoD) MEEP program under Award N00014-19-1-2728 and Bose Family Donation. The authors thank Drs. Keren Lozano and Victoria Padilla for the help with SEM and thank the discussion with and the support from Dr. Enrique Rocha Rangel at the Polytechnic University of Victoria.

Reference

1. Zhang, Y., et al., *Microstructures and properties of high-entropy alloys.* Progress in Materials Science, 2014. **61**: p. 1-93.
2. Tsai, M.-H. and J.-W. Yeh, *High-entropy alloys: a critical review.* Materials Research Letters, 2014. **2**(3): p. 107-123.
3. Cantor, B., et al., *Microstructural development in equiatomic multicomponent alloys.* Materials Science and Engineering: A, 2004. **375**: p. 213-218.
4. Yeh, J.W., et al., *Nanostructured high-entropy alloys with multiple principal elements: novel alloy design concepts and outcomes.* Advanced Engineering Materials, 2004. **6**(5): p. 299-303.
5. Jien-Wei, Y., *Recent progress in high entropy alloys.* Ann. Chim. Sci. Mat, 2006. **31**(6): p. 633-648.
6. Tong, C.-J., et al., *Mechanical performance of the Al x CoCrCuFeNi high-entropy alloy system with multiprincipal elements.* Metallurgical and Materials Transactions A, 2005. **36**(5): p. 1263-1271.
7. Wen, L., et al., *Effect of aging temperature on microstructure and properties of AlCoCrCuFeNi high-entropy alloy.* Intermetallics, 2009. **17**(4): p. 266-269.
8. Singh, S., et al., *Decomposition in multi-component AlCoCrCuFeNi high-entropy alloy.* Acta Materialia, 2011. **59**(1): p. 182-190.
9. Tsai, M.-H., et al., *Morphology, structure and composition of precipitates in Al0. 3CoCrCu0. 5FeNi high-entropy alloy.* Intermetallics, 2013. **32**: p. 329-336.

10. Li, C., et al., *Effect of aluminum contents on microstructure and properties of AlxCoCrFeNi alloys.* Journal of Alloys and Compounds, 2010. **504**: p. S515-S518.
11. Wang, W.-R., et al., *Effects of Al addition on the microstructure and mechanical property of AlxCoCrFeNi high-entropy alloys.* Intermetallics, 2012. **26**: p. 44-51.
12. Chen, M.-R., et al., *Microstructure and properties of Al0. 5CoCrCuFeNiTix (x= 0–2.0) high-entropy alloys.* Materials Transactions, 2006. **47**(5): p. 1395-1401.
13. Zhou, Y., et al., *Solid solution alloys of Al Co Cr Fe Ni Ti x with excellent room-temperature mechanical properties.* Applied physics letters, 2007. **90**(18): p. 181904.
14. Zhang, K., et al., *Microstructure and mechanical properties of CoCrFeNiTiAlx high-entropy alloys.* Materials Science and Engineering: A, 2009. **508**(1-2): p. 214-219.
15. Wang, Y., et al., *Microstructure and compressive properties of AlCrFeCoNi high entropy alloy.* Materials Science and Engineering: A, 2008. **491**(1-2): p. 154-158.
16. Zhu, J.M., et al., *Microstructures and compressive properties of multicomponent AlCoCrFeNiMox alloys.* Materials Science & Engineering: A (Structural Materials: Properties, Microstructure and Processing), 2010. **527**(26): p. 6975-9.
17. Gorr, B., et al., *Phase equilibria, microstructure, and high temperature oxidation resistance of novel refractory high-entropy alloys.* Journal of Alloys and Compounds, 2015. **624**: p. 270-278.
18. Hsu, C.-Y., et al., *Effect of iron content on wear behavior of AlCoCrFexMo0.5Ni high-entropy alloys.* Wear, 2010. **268**(5): p. 653-659.
19. Chen, P., et al., *Fabricating CoCrFeMnNi high entropy alloy via selective laser melting in-situ alloying.* Journal of Materials Science and Technology, 2020. **43**: p. 40-43.
20. Li, N., et al., *Fe-based metallic glass reinforced FeCoCrNiMn high entropy alloy through selective laser melting.* Journal of Alloys and Compounds, 2020. **822**.
21. Tonelli, L., et al., *Effects of powders and process parameters on density and hardness of A357 aluminum alloy fabricated by selective laser melting.* International Journal of Advanced Manufacturing Technology, 2020. **106**(1-2): p. 371-383.
22. Tonelli, L., A. Fortunato, and L. Ceschini, *CoCr alloy processed by selective laser melting (SLM): Effect of laser energy density on microstructure, surface morphology, and hardness.* Journal of Manufacturing Processes, 2020. **52**: p. 106-119.
23. Zhou, R., et al., *Microstructures and mechanical properties of C-containing FeCoCrNi high-entropy alloy fabricated by selective laser melting.* Intermetallics, 2018. **94**: p. 165-171.
24. Luo, S., et al., *Selective laser melting of an equiatomic AlCrCuFeNi high-entropy alloy: Processability, non-equilibrium microstructure and mechanical behavior.* Journal of Alloys and Compounds, 2019. **771**: p. 387-397.
25. Gu, D. and Y. Shen, *Effects of processing parameters on consolidation and microstructure of W–Cu components by DMLS.* Journal of Alloys and Compounds, 2009. **473**(1-2): p. 107-115.
26. Cryosystems, O., *Crystallographica search-match.* Journal of Applied Crystallography, 1999. **32**(2): p. 379-380.
27. Takeuchi, A. and A. Inoue, *Mixing enthalpy of liquid phase calculated by Miedema's scheme and approximated with sub-regular solution model for assessing forming ability of amorphous and glassy alloys.* Intermetallics, 2010. **18**(9): p. 1779-1789.